Proceedings of the ASME 2015 Power and Energy Conversion Conference
PowerEnergy2015
June 28-July 2, 2015, San Diego, California

PowerEnergy2015-49421

CHARACTERIZATION OF PARTICLE FLOW IN A FREE-FALLING SOLAR PARTICLE RECEIVER

Clifford K. Ho,[1] Joshua M. Christian,[1] David Romano,[2] Julius Yellowhair,[1] and Nathan Siegel[3]

[1]Sandia National Laboratories, Albuquerque, New Mexico, 87185-1127, USA, (505) 844-2384, ckho@sandia.gov
[2]Polytechnic University of Turin, Corso Duca degli Abruzzi, 24, 10129 Torino, Italy
[3]Bucknell University, 701 Moore Avenue, Lewisburg, PA 17837

ABSTRACT

Falling particle receivers are being evaluated as an alternative to conventional fluid-based solar receivers to enable higher temperatures and higher efficiency power cycles with direct storage for concentrating solar power applications. This paper presents studies of the particle mass flow rate, velocity, particle-curtain opacity and density, and other characteristics of free-falling ceramic particles as a function of different discharge slot apertures. The methods to characterize the particle flow are described, and results are compared to theoretical and numerical models for unheated conditions.

1. INTRODUCTION

Falling particle receivers are being evaluated to increase operating temperatures and power cycle efficiencies for concentrating solar power applications [1]. In falling particle receivers, small sand-like particles are released through a slot above a cavity receiver, where concentrated sunlight directly irradiates and heats the falling particles. The hot particles are stored and then used to heat the working fluid for the power cycle.

Previous studies have shown that particle flow characteristics vary as a function of slot aperture size, mass flow rate, particle size, and external conditions (e.g., wind) [2, 3]. The particle flow characteristics can subsequently impact particle heating and receiver thermal efficiency [3-5]. The objective of this paper is to characterize the particle flow characteristics of a ~1 MW_t falling particle receiver prototype constructed by Sandia National Laboratories to test and evaluate the performance of high-temperature falling particle receiver designs. Figure 1 shows a schematic of the prototype and its major components, which include the top hopper, the receiver (~2m x 2m x 2m), the bottom hopper, and a particle elevator to recirculate the particles from the bottom hopper back to the top hopper.

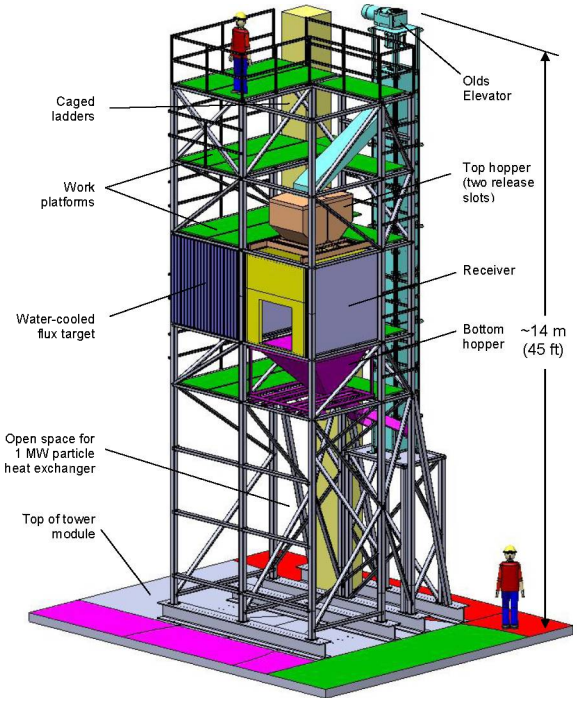

Figure 1. Falling particle receiver prototype.

2. PARTICLE PROPERTIES

The ceramic particles used in the tests were CARBO ACCUCAST ID50. These particles have been shown to have excellent durability under high temperatures and good radiative properties [6-8]. The particle properties are summarized in Table 1.

Table 1. CARBO Accucast ID50 particle properties (from www.carboceramics.com unless otherwise noted)

Property	Value
Mass-median particle diameter (microns)	280
Particle density[1] (kg/m^3)	3300
Loose bulk density at 1100°C (kg/m^3)	1810
Packed bed bulk density at 1100°C (kg/m^3)	2000
Bulk porosity[2] (-)	0.39 (packed) 0.45 (loose)
Packed bed bulk thermal conductivity at 1100°C (W/m-K)	0.7
Particle thermal conductivity[3] at 1100 °C (W/m-K)	2
Specific heat[4] (J/kg-K)	$3657T^{0.18}$ for 50°C ≤ T ≤ 1100°C
Packed-bed solar absorptance[5] (-)	0.91
Packed bed thermal emittance[6] at 700°C (-)	0.75
Sphericity	0.9
Composition	75% Al_2O_3, 11% SiO_2, 9% Fe_2O_3, 3% TiO_2

[1]Measured using Micromeritics AccuPyc 1330 pyncometer (courtesy Andrea Ambrosini, SNL)
[2]Calculated from particle density and loose/packed bulk densities
[3]Calculated using average of series and parallel bulk thermal conductivity models
[4]Fit to data from Netzsch STA 409 (courtesy Eric Coker, SNL)
[5]Measured as-received using Surface Optics 410-Solar. See [8] for degradation at elevated temperatures.
[6]Measured using Surface Optics ET-100 (courtesy James Yuan, SNL)

3. PARTICLE MASS FLOW RATES

3.1. Olds Elevator Mass Flow Rates

The Olds Elevator is used to lift and recirculate particles from the bottom hopper to the top hopper, where the particles are released into the receiver. The elevator procured for Sandia's prototype is rated for operation at ~800°C. The Olds Elevator employs the Archimedes' screw principle; it has a stationary internal screw and a rotating casing around the screw. The rotating casing scoops particles at the base of the screw and lifts the particles along the flights of the screw via friction. The casing speed is controlled by a variable frequency drive (VFD) connected to a 25 HP motor. The mass flow rate from the elevator is a direct function of the frequency of the VFD. Four frequencies (20, 30, 40, and 54 Hz) were evaluated to establish a reference curve for mass flow rate versus frequency. The particle discharge from the top of the Olds Elevator was collected in a hopper suspended by a crane, and a Dillon EDXtreme dynamometer was used to record the mass accumulation as a function of time to determine the mass flow rate. Mass flow measurements at each frequency were repeated three times in random order and the average mass flow rate for each frequency was plotted in Figure 2. Results show that the Olds elevator mass flow rate is a linear function of the VFD setting with a coefficient of determination of 0.99.

After the initial elevator mass-flow measurements were recorded, the top hopper was assembled and a longer duct was added to connect the Olds Elevator discharge chute to the top hopper. Discharge plates placed at the base of the top hopper with different slot aperture sizes could then be characterized.

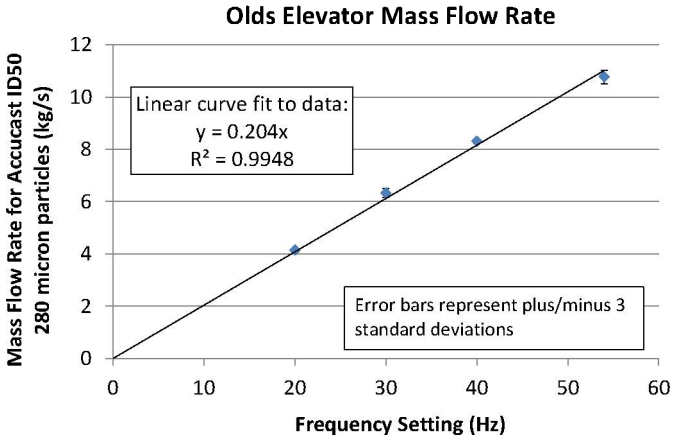

Figure 2. Measured mass flow rate (kg/s) vs. VFD frequency (Hz) in Olds Elevator using CARBO Accucast ID50K ceramic particles with median diameter of 280 microns.

3.2. Mass Flow Rate through Discharge Plate Slot Apertures

While the Olds Elevator could be used to control the mass flow rate of particles released into the receiver, it would be difficult to evenly distribute the particles falling from the top hopper at varying flow rates. Instead, the prototype design for the top hopper uses discharge plates of fixed slot aperture size. The steel plates are removable so that the mass flow rate of the hopper can be varied by selecting different slot apertures. This system is simple, but it is suitable for high temperatures when moving parts (e.g., slide gates) may pose a problem after thermal expansion. The discharge slot apertures evaluated in this study were 6.35, 9.53, 11.1 and 12.7 mm, which correspond to 1/4, 3/8, 7/16, and 1/2 inch, respectively. All slot widths were 1.24 m and the plate thickness was 4.8 mm (3/16 inch). Figure 3 shows the dimensions of the 9.53 mm (3/8 inch) discharge plate.

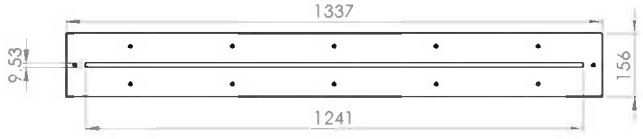

Figure 3. Dimensions (mm) for the 9.53 mm aperture discharge plate.

If the particle elevator supplies a mass flow rate that exceeds the mass flow rate through the discharge plate, particles will accumulate in the top hopper and the particles will be released uniformly along the entire length of the discharge slot. Figure 4 shows an example of particles falling through an 11.1 mm slot aperture, producing a well-defined curtain. The following sections describe models and measurements of particle mass flow rates through varying slot aperture sizes.

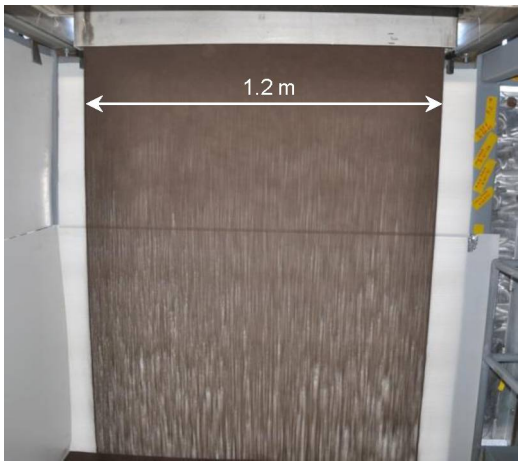

Figure 4. Falling particle curtain released through 11.1 mm (7/16 inch) discharge slot aperture.

3.2.1. Modeling Particle Flow through Apertures

Empirical models have been developed to predict the mass flow rate of granular solids through orifices [9-12]. Janda et al. [11] recommended the following modified form of the Beverloo et al. equation [9]:

$$\dot{m} = C_1 \rho_b \sqrt{g} \left(D - C_2 d\right)^{n+0.5} \quad (1)$$

where

$\dot{m}$ = Mass flow rate (kg/s for 3D or kg/s/m for 2D)
C_1 = Dimensionless constant related to material properties
ρ_b = Bulk density of particles above the aperture (kg/m^3)
g = Gravitational constant (9.81 m/s^2)
D = Aperture size (m)
C_2= Geometrical factor accounting for the effective outpouring section being smaller than the aperture
d = Particle size (m)
n = "1" for 2D and "2" for 3D

Most of the previous studies using forms of Eq. (1) have focused on agricultural products (e.g., seeds). In the next section, we attempt to use Eq. (1) for the alumina-silica ceramic particles investigated in this study and determine appropriate dimensionless constants for C_1 and C_2.

3.2.2. Measured Particle Flow through Apertures

The particle mass flow rate through the different discharge plate slot apertures was measured by setting the Olds Elevator to a high particle flow rate (greater than the mass flow rate through the slot aperture of the discharge plate in the top hopper). The top hopper accumulated with particles until the entire slot width had a steady flow of particles. The particles that flowed through the aperture were then collected and weighed as a function of time to determine the mass flow rate. The process was repeated for each of the different discharge plates.

Figure 5 shows the results of the measured particle mass flow rates as a function of discharge slot aperture for two different particle sizes. The current study evaluated the 280 micron particles, while the data for the 697 micron particles were obtained from Siegel et al. [4]. The predicted mass flow rates using Eq. (1) are also plotted in Figure 5 assuming a packed bulk density of 2,000 kg/m^3 and fitted values for C_1 and C_2. The particle mass flow rate increases rapidly as the slot aperture increases and decreases as the particle size increases.

The root-sum-squared error between the predicted mass flow rates and the measured mass flow rates as a function of slot aperture size and two different particles sizes was minimized when C_1 = 62 and C_2 = 1.4. The fit between the data and the model predictions is excellent within the range of the measured values. Thus, Eq. (1) can be used to estimate mass flow rates of ceramic particles as a function of slot aperture and particle size. It is interesting to compare the fitted values of C_1 (62) and C_2 (1.4) for the ceramic particles used in this study with the corresponding values (35 and 1.4, respectively) found in Beverloo et al. [9] for agricultural granular solids (e.g., seeds).

It should be noted that the maximum mass flow rate of the Olds Elevator was less than the capacity of the 12.7 mm (0.5 inch) slot aperture for 280 micron particles (as evidenced by particles not accumulating in the top hopper nor covering the entire length of the aperture). Therefore, the maximum flow rate shown in Figure 5 is for the 11.1 mm (7/16 inch) slot aperture.

4. PARTICLE VELOCITY

4.1. Particle Velocity Modeling

For a particle released from rest, the velocity, v (m/s), as a function of time, t (s), and free-fall distance, y (m), can be expressed as follows by integrating Newton's 2nd law of motion, assuming no drag:

$$v(t) = gt \quad (2)$$

$$v(y) = \sqrt{2gy} \quad (3)$$

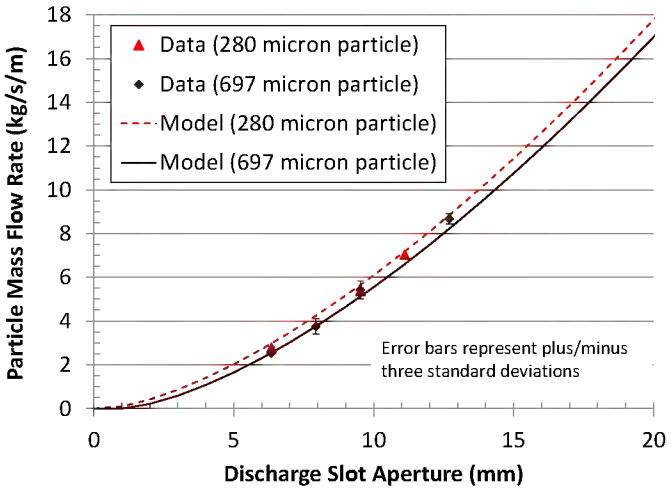

Figure 5. Measured and modelled mass flow rates as a function of different discharge slot apertures for 280 and 697 micron particle sizes.

If air resistance (drag) is present, the following expressions can be used to determine the velocity as a function of time and position:

$$v(t) = v_\infty \tanh\left(\frac{gt}{v_\infty}\right) \tag{4}$$

$$y(t) = \frac{v_\infty^2}{g} \ln\left(\cosh\left(\frac{gt}{v_\infty}\right)\right) \tag{5}$$

$$v_\infty = \sqrt{\frac{2mg}{\rho_{air} C_d A}} \tag{6}$$

where v_∞ is the terminal velocity (m/s), m is the mass of the particle (3.79e-8 kg), ρ_{air} is the air density (1.2 kg/m^3 at 15°C), A is the cross-sectional area of the particle (6.16e-8 m^2), and C_d is the coefficient of drag for a sphere (solved iteratively as a function of Reynolds number; C_d=2.84, Re=36, v_∞=1.88 m/s).

Simulations of free-falling particles released through a slot aperture were also performed using ANSYS Fluent 15.0. The Discrete Phase Model (DPM) was used to simulate particles released from slot apertures of prescribed dimensions corresponding to the test articles. The DPM simulates particle motion in a Lagrangian reference frame governed by a force balance on the particle. The force balance includes a drag force that accounts for the velocity of the particle, velocity of the surrounding fluid, particle size, and fluid properties [13]. The velocity at various drop distances was recorded, along with the particle width, thickness, and concentration. A total of ~1 million hexahedral elements were used in the model, which consisted of a cubical domain with a slot aperture in the middle of the top surface, walls on the side, and a pressure opening at the bottom. The slot surface consisted of 300 x 20 elements. A grid independence study was performed to ensure that the resolution of the grid was sufficient. Figure 6 shows the results of a Fluent simulation of particle flow (280 micron particle diameter) when released from a 9.53 mm slot aperture.

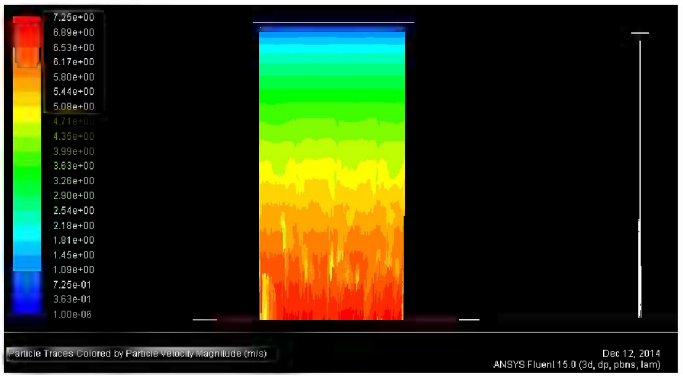

Figure 6. Ansys Fluent simulation of the falling particle curtain velocity with a 9.53 mm (3/8 inch) slot aperture. Particle traces are colored by velocity magnitude.

4.2. Particle Velocity Measurements

The velocity distribution of particles falling through the discharge plates were measured using a high-speed camera (Allied Vision Technologies NX4-S1) with images recorded every 1/200th second. Rather than using particle image velocimetry, which requires lasers or high-powered lights, we analyzed visible features in successive images of the falling particle curtain. The movement of the features were tracked, and the distance the features moved in subsequent images was then divided by the time between images to obtain the velocity at various locations of the particle curtain. Several locations near the top, middle, and bottom of the particle curtain were evaluated, and at least three features were tracked at each location to quantify the uncertainty in the measurements.

Figure 7 shows three successive images of the falling particles for the 9.53 mm slot aperture. The letters (A, B, C, and D) denote the relative locations of the features that were tracked, which are outlined in red. A spatial reference scale that was visible in each image was used to track the distance traveled. The number ("1") refers to the set of features that was tracked in these images. Additional sets of features were tracked in these and other images.

The measured, simulated, and analytically modelled particle velocities as a function of distance from release are plotted in Figure 8. Results show that the measured and simulated particle velocities align closely with the analytical predictions of a single falling particle assuming no drag (see Eq. (3)). Analytical predictions of a single falling particle (280 μm) with drag yielded velocities (terminal velocity = 1.88 m/s) that were substantially lower than the measured and simulated velocities. The reason for the discrepancy is the downward entrainment of air by the large number of particles falling as a curtain through the receiver. The resulting downward bulk flow of air minimizes the air resistance on individual particles.

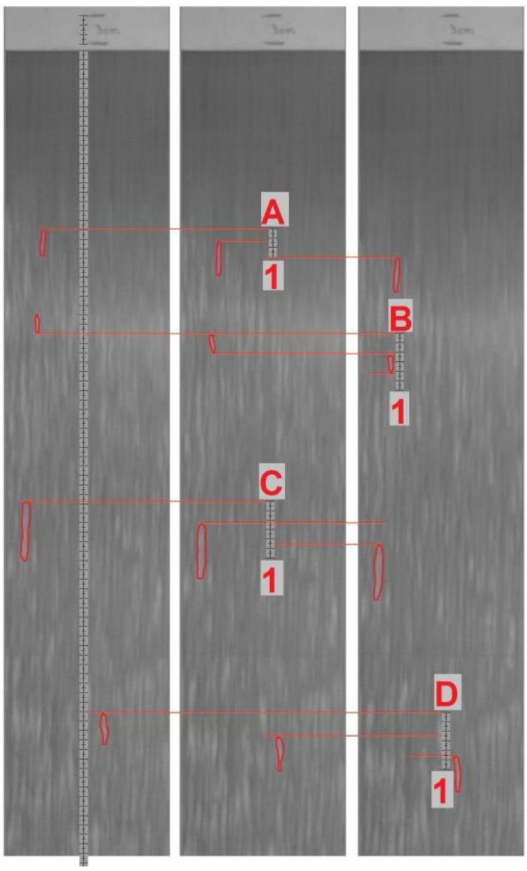

Figure 7. Successive high-speed images of the falling particle curtain (280 micron median particle size) with a 9.53 mm (3/8 inch) slot aperture used to determine particle velocities. Each image was taken 1/200 seconds apart.

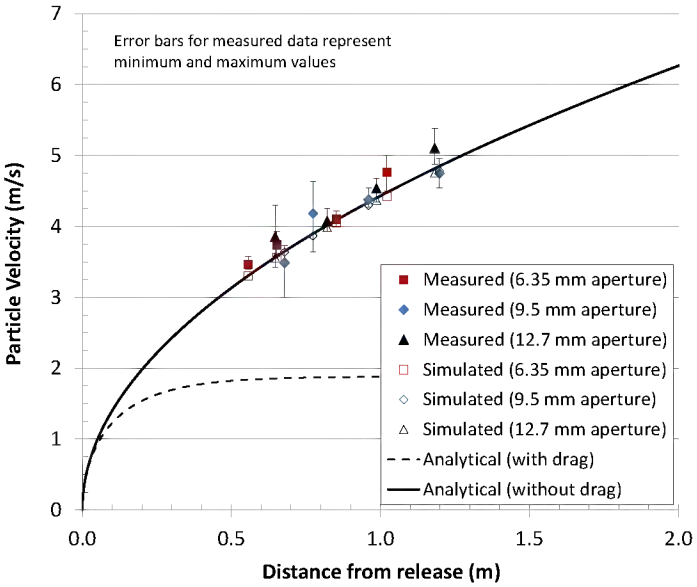

Figure 8. Measured, simulated (Ansys Fluent), and analytically modelled particle velocities.

5. PARTICLE CURTAIN PROPERTIES

5.1. Particle Curtain Thickness and Width

The measured and simulated width of the particle curtain for the 6.35, 9.53, and 11.1 mm slot apertures was nearly constant at 1.2 m (see Figure 4 and Figure 6). The mass flow rate through the 12.7 mm slot aperture exceeded the maximum mass flow rate of the Olds Elevator, so a uniform particle release across the entire width of the discharge slot could not be obtained. The thickness of the particle curtain generally increased with distance from the release point. Figure 9 shows three side-view images of the particle curtain discharged from three different slot aperture sizes. A white poster board with length scales was placed within the particle curtain to better visualize the curtain thickness associated with a short section of the particle curtain. The board also reduced the effects from parallax and waviness along the particle curtain.

Figure 10 shows the measured and simulated particle curtain thickness for three different slot apertures as a function of distance from release. The simulated results show that the curtain thickness actually decreases from the point of release to ~1 – 2 m, but then increases with increasing drop distances. This could be due to the Bernoulli principle, in which the increasing velocities of the falling particles reduce the air pressure near the center of the particle curtain, which pulls air in from outside the curtain and may push the particles together. As the particles continue to fall, particle collisions may cause the particles to spread and offset the Bernoulli effect.

The measured particle-curtain thicknesses ranged from ~1 – 3 cm over the length of the receiver (1 – 2 m) and are larger than the simulated thicknesses for the different slot apertures. We postulate that this may be caused by a couple factors. First, the particles that fall through the discharge slot can have some horizontal momentum as the particles move downward and sideways within the accumulated pile toward the slot. The simulations assumed that the particles were released from rest. The initial horizontal momentum would cause additional spreading and increased particle curtain thickness. Second, the presence of the bottom hopper caused the entrained downward air flow to be redirected upward when the particles reached the bottom hopper. This upward flow of air may have caused additional disruptions in the air flow near the curtain, which increased the curtain thickness. The bottom hopper was not included in the simulations.

Figure 9. Side view of particle curtain thicknesses for 280 micron particles falling through three different slot apertures: 6.35 mm (left), 9.53 mm (middle), and 11.1 mm (right). Hash marks are 1 cm apart.

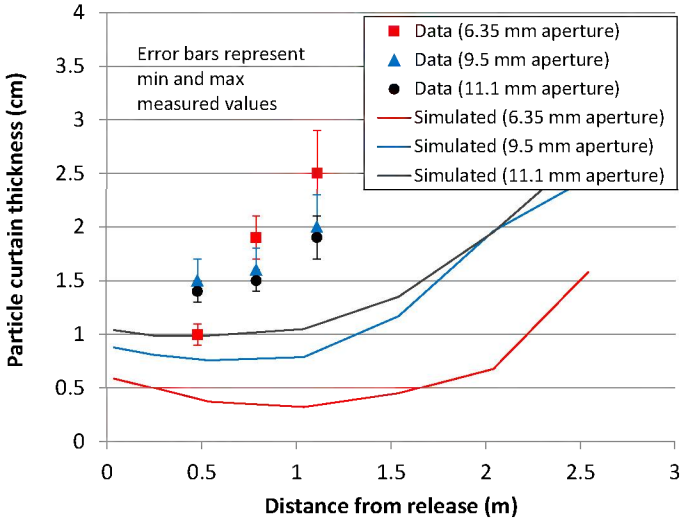

Figure 10. Measured and simulated particle curtain thickness as a function of drop distance.

5.2. Falling Particle Volume Fraction

The particle bulk density (particle mass per total bulk volume) in the falling particle curtain, $\rho_{b,f}$, can be calculated as a function of drop distance, y, from the definition of the mass flow rate:

$$\rho_{b,f}(y) = \frac{\dot{m}}{v(y)A(y)} \tag{7}$$

The mass flow rate, $\dot{m}$ (kg/s), for the 280 micron particles was obtained from the measurements described in Section 3.2.2. Eq. (3) was used to analytically express the velocity as a function of drop distance since the simulations and data showed good agreement to the analytical model (assuming no drag) for all slot apertures. The cross-sectional area of the particle curtain, $A(y)$, was calculated as the product of the width and thickness of the curtain described in Section 5.1.

The particle volume fraction (ratio of particle volume to total volume) within the falling particle curtain is calculated by dividing the particle bulk density of the curtain defined in Eq. (7) by the particle density (3300 kg/m^3). The measured and simulated particle volume fractions for different slot apertures are shown in Figure 11. The initial particle volume fraction can be calculated as the particle packed bed density (2000 kg/m^3) divided by the particle density, which yields ~0.6 or 60%. As the particles fall, the particle volume fraction decreases rapidly. The particle volume fraction decreases to less than 10% at drop distances greater than ~0.5 m from the release point due to the rapidly increasing velocity, which spreads out the particles in the vertical direction. The cross-sectional area also changes with increasing distance, although the change is relatively small within the drop distances spanned by the receiver in this study (~1 – 2 m). The measured particle volume fractions are lower than the simulated values due to the larger measured curtain thicknesses shown in Figure 10 and as discussed in Section 5.1.

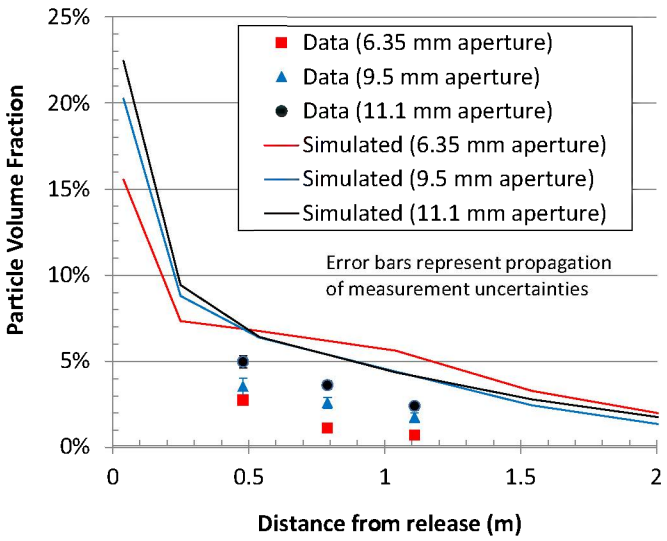

Figure 11. Measured and simulated particle volume fraction as a function of drop distance for different slot apertures and a median particle size of 280 microns.

5.3. Particle Curtain Transmittance/Opacity

The transmittance of the particle curtain is defined as the fraction of light incident on the curtain that passes through the particle curtain. The opacity of the particle curtain, defined as the ratio of incident light intercepted by the particles to the total amount of light incident on the curtain, can be calculated as one minus the transmittance. The transmittance was measured in two different ways. First, a Lux meter (LX1330B) was placed

both behind and in front of the particle curtain, facing towards a fixed light source, along three vertical locations of the curtain. The ratio of the Lux readings gave the light transmittance through the curtain. Second, photographs were taken with and without the particle curtain present in ambient backlighting. The ratio of the pixel values in the two images with and without the particle curtain also gave the light transmittance. The advantage of this second method is that it provides a continuous measurement of the transmittance (and opacity) throughout the entire field of view. Figure 12 shows sample images using the photographic method.

Figure 13 shows the measured opacity as a function of drop distance for three different slot apertures using both measurement methods. The measured values began at a distance of ~0.5 m from the release point since a ~46 cm discharge chute extended from the discharge plate into the receiver. In the photographic method, the opacity was averaged along each row of pixels in the particle-curtain image, and error bars were plotted to represent one standard deviation. The opacity of the particle curtain is quite high for all three slot apertures near the release point. For the 9.53 mm and 11.1 mm slot apertures, the opacity of the particle curtain is above 95% within ~0.7 m of the release point. For the 6.35 mm aperture, the opacity is ~80% within ~0.6 m of the release point. The opacity decreases with increasing distance as the particles spread apart with increasing velocity and curtain thickness.

6. CONCLUSIONS

A particle flow characterization study has been performed on ceramic particles for a prototype falling particle receiver. These studies and results will help to inform models and on-sun heating tests of falling particle receivers for concentrating solar power applications. The following conclusions can be drawn from this study:

6.1. Particle mass flow rates

- The particle mass flow rate increases with increasing slot aperture sizes according to a power law.
- Smaller particles yield a greater mass flow rate than larger particles for a given aperture size.
- The measured mass flow rates for two particle sizes were matched well with predictions from a modified Beverloo equation (see Section 3.2.1).
- The mass flow rate of the Olds Elevator exhibited a linear correlation (R^2=0.99) with the drive frequency. The maximum mass flow rate of the Olds Elevator exceeded the mass flow rate through the 6.35, 9.53, and 11.1 mm slot apertures, but it could not exceed the flow rate through the 12.7 mm slot aperture.

6.2. Particle velocities

- The measured and simulated particle velocities as a function of distance from the release point were predicted by the analytical free-fall model assuming no drag. Particle entrainment of air reduced the drag.

6.3. Particle curtain properties

- The particle curtain width remained nearly constant along the drop length of the receiver.
- The particle thickness varied with drop distance.
  - Simulated curtain thicknesses exhibited a minimum ~1 m from the release point, perhaps from the Bernoulli effect.
  - Measured curtain thicknesses were generally larger than the simulated values due to initial horizontal momentum of the particles at the release point and an updraft of air caused by the bottom hopper.

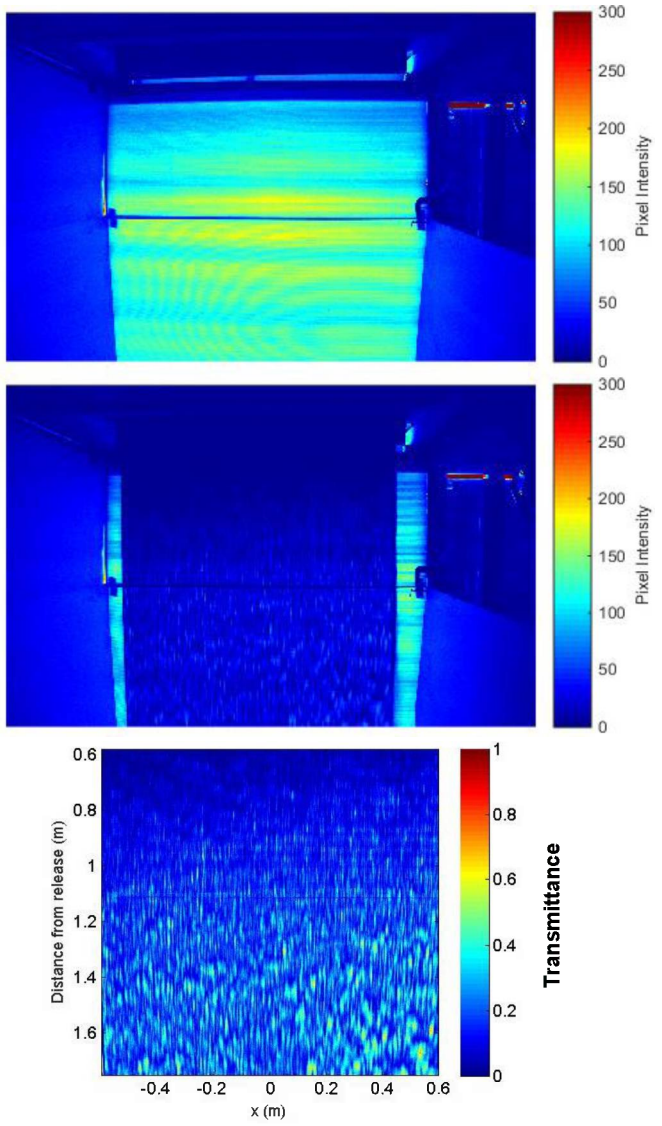

Figure 12. Top: raw image without particle curtain. Middle: raw image with particle curtain (9.53 mm aperture, 280 μm particles). Bottom: ratio of images with and without particle curtain yielding transmittance (one minus opacity), cropped over the particle curtain.

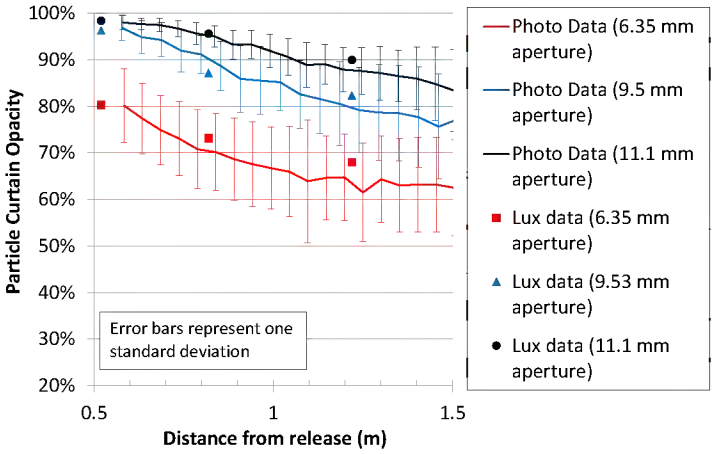

Figure 13. Measured particle-curtain opacity (one minus transmittance) as a function of drop distance for different slot apertures and 280 micron particles.

- The particle volume fraction in the curtain decreased rapidly from a theoretical value of 60% at the release point to less than 10% within 0.5 m of drop distance.
- The particle curtain opacity was greater than 95% within ~0.7 m of the release point for the 9.53 and 11.1 mm slot apertures and decreased steadily with increasing distance. The particle curtain opacity was ~80% within ~0.6 m of the release point for the 6.35 mm slot aperture.

ACKNOWLEDGEMENTS

The authors acknowledge Daniel Ray, JJ Kelton, Doug Robb, Eric Coker, Andrea Ambrosini, and James Yuan for their assistance with the particle characterization tests. Sandia National Laboratories is a multi-program laboratory managed and operated by Sandia Corporation, a wholly owned subsidiary of Lockheed Martin Corporation, for the U.S. Department of Energy's National Nuclear Security Administration under contract DE-AC04-94AL85000. The United States Government retains and the publisher, by accepting the article for publication, acknowledges that the United States Government retains a non-exclusive, paid-up, irrevocable, world-wide license to publish or reproduce the published form of this manuscript, or allow others to do so, for United States Government purposes.

REFERENCES

[1] Ho, C., J. Christian, D. Gill, A. Moya, S. Jeter, S. Abdel-Khalik, D. Sadowski, N. Siegel, H. Al-Ansary, L. Amsbeck, B. Gobereit, and R. Buck, 2014, Technology advancements for next generation falling particle receivers, *Proceedings of the Solarpaces 2013 International Conference*, **49**(Energy Procedia), p. 398-407.

[2] Ho, C.K., J.M. Christian, A.C. Moya, J. Taylor, D. Ray, and J. Kelton, 2014, *Experimental and Numerical Studies of Air Curtains for Falling Particle Receivers*, in *Proceedings of ASME 2014 8th International Conference on Energy Sustainability*, ES-FuelCell2014-6632, Minneapolis, MN, June 29 - July 2, 2014.

[3] Siegel, N., G. Kolb, K. Kim, V. Rangaswamy, and S. Moujaes, 2007, Solid particle receiver flow characterization studies, *Proceedings of the Energy Sustainability Conference 2007*, p. 877-883.

[4] Siegel, N.P., C.K. Ho, S.S. Khalsa, and G.J. Kolb, 2010, Development and Evaluation of a Prototype Solid Particle Receiver: On-Sun Testing and Model Validation, *Journal of Solar Energy Engineering-Transactions of the Asme*, **132**(2).

[5] Ho, C.K., S.S. Khalsa, and N.P. Siegel, 2009, *Modeling on-Sun Tests of a Prototype Solid Particle Receiver for Concentrating Solar Power Processes and Storage*, in *ES2009: Proceedings of the ASME 3rd International Conference on Energy Sustainability, Vol 2*, San Francisco, CA,

[6] Knott, R., D.L. Sadowski, S.M. Jeter, S.I. Abdel-Khalik, H.A. Al-Ansary, and A. El-Leathy, 2014, *High Temperature Durability of Solid Particles for Use in Particle Heating Concentrator Solar Power Systems*, in *Proceedings of the ASME 2014 8th International Conference on Energy Sustainability*, ES-FuelCell2014-6586, Boston, MA, June 29 - July 2, 2014.

[7] Knott, R., D.L. Sadowski, S.M. Jeter, S.I. Abdel-Khalik, H.A. Al-Ansary, and A. El-Leathy, 2014, *Sintering of Solid Particulates under Elevated Temperature and Pressure in Large Storage Bins for Thermal Energy Storage*, in *Proceedings of the ASME 2014 8th International Conference on Energy Sustainability*, ES-FuelCell2014-6588, Boston, MA, June 29 - July 2, 2014.

[8] Siegel, N., M. Gross, C. Ho, T. Phan, and J. Yuan, 2014, Physical properties of solid particle thermal energy storage media for concentrating solar power applications, *Proceedings of the Solarpaces 2013 International Conference*, **49**(Energy Procedia), p. 1015-1023.

[9] Beverloo, W.A., H.A. Leniger, and J. Vandevelde, 1961, The Flow of Granular Solids through Orifices, *Chemical Engineering Science*, **15**(3-4), p. 260-&.

[10] Fowler, R.T. and J.R. Glastonbury, 1959, The Flow of Granular Solids through Orifices, *Chemical Engineering Science*, **10**(3), p. 150-156.

[11] Janda, A., I. Zuriguel, and D. Maza, 2012, Flow Rate of Particles through Apertures Obtained from Self-Similar Density and Velocity Profiles (vol 108, 248001, 2012), *Physical Review Letters*, **109**(18).

[12] Harmens, A., 1963, Flow of Granular Material through Horizontal Apertures, *Chemical Engineering Science*, **18**(5), p. 297-306.

[13] Morsi, S.A. and Alexande.Aj, 1972, Investigation of Particle Trajectories in 2-Phase Flow Systems, *Journal of Fluid Mechanics*, **55**(Sep26), p. 193-&.